

Challenges and Constraints of Using Oxygen Cathodes in Microbial Fuel Cells

FENG ZHAO,[†] FALK HARNISCH,[†]
UWE SCHRÖDER,^{*,†} FRITZ SCHOLZ,[†]
PETER BOGDANOFF,[‡] AND
IRIS HERRMANN[‡]

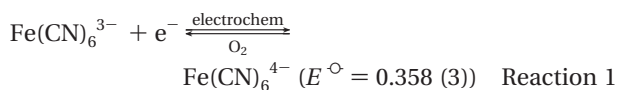
Institut für Chemie und Biochemie, Universität Greifswald, Soldmannstrasse 16, 17489 Greifswald, Germany, and Hahn-Meitner-Institut Berlin, Glienicke Strasse 100, 14109 Berlin, Germany.

The performance of oxygen reduction catalysts (platinum, pyrolyzed iron(II) phthalocyanine (pyr-FePc) and cobalt tetramethoxyphenylporphyrin (pyr-CoTMPP)) is discussed in light of their application in microbial fuel cells. It is demonstrated that the physical and chemical environment in microbial fuel cells severely affects the thermodynamics and the kinetics of the electrocatalytic oxygen reduction. The neutral pH in combination with low buffer capacities and low ionic concentrations strongly affect the cathode performance and limit the fuel cell power output. Thus, the limiting current density in galvanodynamic polarization experiments decreases from 1.5 mA cm⁻² to 0.6 mA cm⁻² (pH 3.3, $E_{\text{cathode}} = 0$ V) when the buffer concentration is decreased from 500 to 50 mM. The cathode limitations are superposed by the increasing internal resistance of the MFC that substantially contributes to the decrease of power output. For example, the maximum power output of a model MFC decreased by 35%, from 2.3 to 1.5 mW, whereas the difference between the electrode potentials ($\Delta E = E_{\text{anode}} - E_{\text{cathode}}$) decreased only by 10%. The increase of the catalyst load of pyr-FePc from 0.25 to 2 mg cm⁻² increased the cathodic current density from 0.4 to 0.97 mA cm⁻² (pH 7, 50 mM phosphate buffer). The increase of the load of such inexpensive catalyst thus represents a suitable means to improve the cathode performance in microbial fuel cells. Due to the low concentration of protons in MFCs in comparison to relatively high alkali cation levels (ratio $c_{\text{Na}^+, \text{K}^+} / c_{\text{H}^+} = 5 \times E5$ in pH 7, 50 mM phosphate buffer) the transfer of alkali ions through the proton exchange membrane plays a major role in the charge-balancing ion flux from the anodic into the cathodic compartment. This leads to the formation of pH gradients between the anode and the cathode compartment.

Introduction

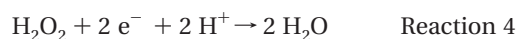
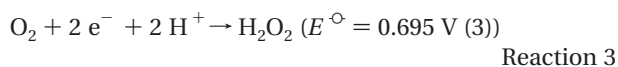
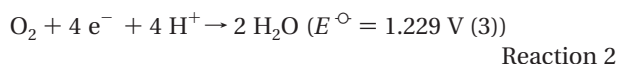
The reduction of molecular oxygen is doubtless the best choice for the cathodic reaction not only for chemical fuel cells, but also for microbial fuel cells. The direct and virtually

inexhaustible availability of oxygen as well as its positive redox potential are two of the major reasons for the superiority of this element as an electron acceptor. The improvement of the performance of the oxygen reduction at lowest possible costs of the cathode material represents one of the most important issues for research and development since it is often the cathodic reaction that limits the performance of, e.g., polymer electrolyte membrane fuel cells and also solid oxide fuel cells (1, 2). Although microbial fuel cells with their comparably low current and power output, which lies orders of magnitude below that of conventional PEM fuel cells, on a first glance would not appear to share the same problem. Yet, it becomes obvious that this exactly is the case. Experimental cathode systems, based on the reduction of hexacyanoferrate(III) ions (Reaction 1), are not sustainable (no sufficient



reoxidation of hexacyanoferrate(II) by oxygen) and have to be replenished regularly (4). Platinum is the best known oxygen reduction catalyst. It becomes increasingly expensive though, and needs to be either substituted by cheaper, nonnoble metal catalysts or to be reduced in the amount at the cathode (catalyst load) (5–7). As an example, Cheng et al. have reduced the platinum load down to 0.1 mg cm⁻², apparently without affecting the MFC performance (5). These data will be discussed later in more detail.

Transition metal porphyrin and phthalocyanine based catalysts show good performance toward oxygen reduction under alkaline (8, 9) and acidic (10–12) conditions. Depending on their ring structure, the nature of the metal ion and the nature of the substituents the oxygen reduction may proceed either directly to water in a four electron reaction (Reaction 2), or it may proceed in a two-step reaction via hydrogen peroxide as the intermediate (Reactions 3, 4), see, e.g., ref 13.



Some complexes are not capable of oxidizing H₂O₂ at sufficient rates. In this case, the reduction stops after the first two electron reduction steps. Hydrogen peroxide, produced as an intermediate or the end product of the oxygen reduction, is known to cause degradation of the transition metal complexes (13).

To improve the catalytic activity and stability of transition metal porphyrin and phthalocyanine catalysts, different strategies have been followed. The polymerization of the metal complexes (14) and the embedding into conductive polymers (15, 16) have been reported. The most promising approach appears to be a pyrolytic heat treatment in an inert atmosphere, which leads to an embedding of the catalytic metal centers into a conductive carbon matrix (17–25). As we have recently shown for the example of pyrolyzed iron(II) phthalocyanine and cobalt tetramethoxyphenylporphyrin

* Corresponding author phone: +49-3834-864330; fax: +49-3834-864451; e-mail: uweschr@uni-greifswald.de.

[†] Institut für Chemie und Biochemie, Universität Greifswald.

[‡] Hahn-Meitner-Institut Berlin.

based oxygen reduction catalysts (26), and as it was confirmed by other researchers (5, 27), these materials are suitable candidates for MFC application.

The conditions for an efficient oxygen reduction in microbial fuel cells are not ideal, and they differ significantly from those present in conventional fuel cells. Ambient temperature, low concentrations of the supporting electrolytes (28), as well as the mostly neutral pH put thermodynamic as well as kinetic constraints on the performance of the MFC cathode (29). In this fundamental study we have investigated the influence of the composition of the cathodic electrolyte solution on the electrocatalytic oxygen reduction reaction. We have studied noble-metal free pyrolyzed iron(II) phthalocyanine (pyr-FePc) and cobalt tetramethoxyphenylporphyrin (pyr-CoTMPP) catalysts in comparison with platinum by means of galvanodynamic, potentiostatic and fuel cell experiments. To study and analyze performance bottlenecks and their origins and to derive possible solutions, systematic variations of electrolyte solution were made—even toward conditions that may not be found in MFC applications (acidic pH, high buffer capacities). Such an approach is useful and necessary to reveal variables for the improvement of the cathode performance and to provide the basis for the development of efficient MFC cathodes. The optimization of the cathode preparation (the choice of binder (5), the binder/catalyst ratio, the catalyst processing etc.) was beyond the scope of this study and should be the focus of further, technological investigations.

Experimental Section

Catalyst Preparation. *Pyrolyzed Iron(II) Phthalocyanine Catalyst (pyr-FePc).* Two g iron(II) phthalocyanine were dissolved in tetrahydrofuran (THF) at room temperature, afterward the mixture was added to a dispersion of 2 g carbon nanoparticles (Vulcan XC-72) in THF, and was treated in an ultrasonic bath for 30 min. Finally, the THF was removed, and subsequently the impregnated carbon nanoparticles were heat treated under argon gas at 700 °C for 2 h. Then this material was ball-milled for 1 h (26).

Pyrolyzed CoTMPP Catalyst (pyr-CoTMPP). The catalyst was prepared from a mixture of CoTMPP (cobalt tetramethoxyphenylporphyrin), iron(II) oxalate and elementary sulfur in a heat treatment procedure under inert gas atmosphere and a subsequent washing in hydrochloric acid in order to remove catalytic inactive byproducts. The detailed preparation method is described in refs 24,30.

Electrode Preparation. The cathode material was graphite foil (Chempur, Karlsruhe, Germany) or carbon cloth (Toray, EC-CCL-060). For galvanostatic half cell experiments graphite foils with an active surface area of 1 cm² were used.

Depending on the catalyst used, different electrode preparation procedures were applied: pyr-FePc was mixed with a carbon support (Vulcan XC 72) in a ratio of 1:1 prior to the electrode modification. This mixture was found to yield the best performance. All catalyst loads in this manuscript refer to the undiluted pyr-FePc. Pyr-CoTMPP was used as prepared since the carbon support is formed during the catalyst synthesis (24). When platinum served as catalyst either commercial carbon supported platinum (20% E-TEK HP Pt on Vulkan XC-72, purchased from DE NORA, Germany) or platinized platinum was used. The total catalyst load of the carbon supported catalyst was 2 mg cm⁻², corresponding to a platinum load of 0.4 mg cm⁻², which is similar to other studies in the field (31).

The electrocatalyst was mixed with poly(tetrafluoroethylene) (Aldrich, 60% dispersion in water) in a ratio of approximately 10 μL PTFE solution to 1 mg catalyst in an ultrasonic bath, the mixture was then transferred onto the substrates and was allowed to dry at 80 °C overnight (26).

Electrolyte Solutions. All electrolyte solutions were prepared using deionized water. All chemicals (NaH₂PO₄, Na₂HPO₄, H₃PO₄, KNO₃, HNO₃, NaOH) were purchased from Aldrich, Fluka, and Merck and were of analytical grade. Oxygen (Messer, Germany, purity >99.5%) or air was purged into the cathode compartment in order to supply the oxygen needed for the electrochemical reaction.

Electrochemical Instrumentation. Cyclic voltammetry and galvanodynamic linear sweep voltammetry were carried out in a conventional three electrode arrangement using Autolab systems (PGSTAT 20, PGSTAT 30, EcoChemie, Netherlands). The reference electrode was a Ag/AgCl electrode (sat. KCl, Sontorteknik Meinsberg, Germany, 0.195 V vs SHE), a platinum sheet served as the counter electrode. These experiments were carried out at room temperature.

Rotating electrode experiments were performed using a 616 EG&G rotating electrode module equipped with a self-made electrode holder that allowed us to clamp graphite foil electrodes (2 cm length, 1 cm width, with 1 cm² active surface area) vertically and axially symmetrically. This setup may be difficult to mathematically describe with respect to the limiting current density, and turbulences are likely to occur. Yet, this modified setup of rotating disk experiments enables the study of electrode materials such as carbon paper or carbon cloth that are difficult to study otherwise. To keep turbulences low, we used comparably low rotation speeds (100 rpm).

The galvanodynamic polarization experiments were performed with a scan rate of 10 μA s⁻¹. For the determination of exchange current densities a slower scan rate (0.1 μA s⁻¹) was used to ensure steady-state conditions and exclude any transient effects. The exchange current density was derived from the Tafel plot obtained from the rotating electrode experiments. We did not study the electrode performance below a potential of zero volts (versus Ag/AgCl). Apart from fuel cell performance reasons, this is due to the observation that a polarization of the transition metal porphyrin and phthalocyanine catalysts below that value leads to a slow recovery of the material. Thus, when polarized to potentials below 0 V in pH neutral solutions, the recovery of the open circuit potential took between 15 and 30 min.

Current and potential measurements in the fuel cell experiments were carried out using a digital multimeter (Integra 2700 series equipped with 7700 multiplexer, Keithley Instruments, Inc., Cleveland, U.S.A.) interfaced to a personal computer. For the determination of the power output a variable resistance (0–60 KΩ) was used as the external load. The current and potential values were taken only when steady-state conditions had established after changing the external resistance. This took up to fifteen minutes at lower resistances.

MFC Test System Setup. For the MFC experiments we used *Escherichia coli* K12 as the biocatalyst (32). Via mixed fermentation this biocatalyst produces hydrogen, which served as the electron carrier in the anode compartment. *Escherichia coli* were grown aerobically at 37 °C for 12–24 h in a standard medium containing 10 g glucose, 5 g yeast extract, 10 g NaHCO₃, and 8.5 g NaH₂PO₄ per liter. The same medium served as the solution in the anode chamber. For the experiments 1 mL of an overnight culture was inoculated into fresh medium, then *E. coli* were cultivated in the anaerobic anode chamber.

The solution in the cathode chamber was a phosphate buffer, either 50 or 500 mM, adjusted to pH 7. Air was purged into the cathode compartment in order to supply the oxygen needed for the electrochemical reaction.

The MFC experiments were carried out in batch mode using a self-made fuel cell model (Figure 4), which was composed of two 250 mL volume-bottom flasks pressed together at laterally inserted windows (33). A Nafion 117

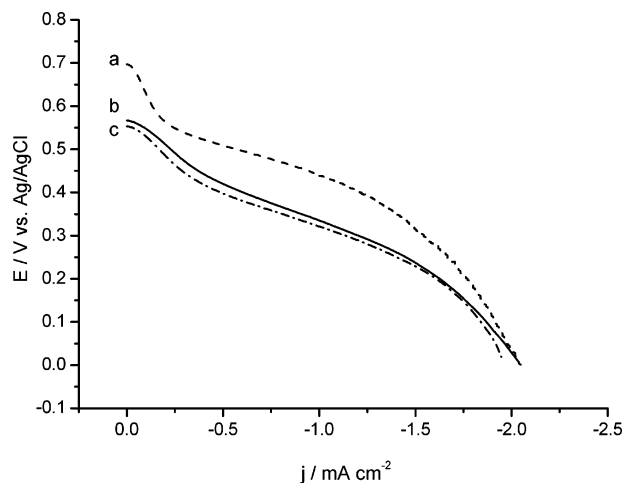


FIGURE 1. Galvanodynamic polarization plots of the electrocatalytic oxygen reduction at (a) platinumized platinum, (b) pyr-CoTMPP, and (c) pyr-FePc modified graphite foil in oxygen saturated solution (0.5 M NaH_2PO_4 , pH 2.4). The solution was stirred and permanently purged with O_2 . The scan rate was 10^{-5} A s^{-1} .

proton exchange membrane (purchased from Aldrich) of 2.2 cm diameter was clamped between the windows separating anode and cathode compartment. The anode was a 100 cm^2 poly(tetrafluoroaniline) coated platinum mesh (34), the cathode was a 60 cm^2 pyr-FePc modified graphite foil (1 $\text{mg}_{\text{pyr-FePc}}/\text{cm}^2$). Both, anode and cathode chamber, contained a reference electrode (Ag/AgCl sat. KCl, 0.195 V vs SHE) for an independent recording of the individual electrode potentials. The MFCs were placed in a temperature-controlled chamber and run at 37 °C. The model MFC, as shown in Figure 4, is well suited for fundamental and mechanistic MFC studies, since it allows a fast and simple fuel cell assembly and electrode replacement. The use of two reference electrodes helps to analyze fuel cell results and reveal performance bottlenecks.

Results and Discussion

Figure 1 shows the results of galvanodynamic linear sweep polarization measurements of the electrocatalytic oxygen reduction at pyr-CoTMPP and pyr-FePc in comparison to platinumized platinum in oxygen saturated acidic (pH 2.4) 0.5 M phosphate buffer. The platinum black electrode showed the highest open circuit potential (697 mV), followed by pyr-CoTMPP and pyr-FePc with 567 mV and 553 mV, respectively. As known from the literature (25), the electrocatalytic oxygen reduction at metal porphyrins and phthalocyanines is often incomplete and leads, to some extent, to the formation of hydrogen peroxide (Reaction 3). The superposition of the Reactions 2 and 3 may thus explain the lower redox potential at the pyr-CoTMPP and pyr-FePc electrodes.

Clearly visible in Figure 1 is the mass transfer limitation that levels the performance of all catalyst materials at current densities above approximately 1.5 mA cm^{-2} . As shown, current densities of 2 mA cm^{-2} are achieved for all catalysts at a cathode potential of 0 V.

Effects of Solution pH. Microbial fuel cells are generally operated at neutral or only slightly acidic pH and considerably lower electrolyte concentrations. Figure 2 shows the effect of a variation of the pH on the electrocatalytic oxygen reduction at a pyr-CoTMPP coated electrode. Clearly visible is the major disadvantage of the oxygen reduction in comparison to the reduction of ferricyanide. Whereas the latter reaction (Reaction 1) and thus its redox potential are independent of the proton concentration, the oxygen reduction reactions involve the consumption of one proton per transferred electron, independently if the reaction proceeds

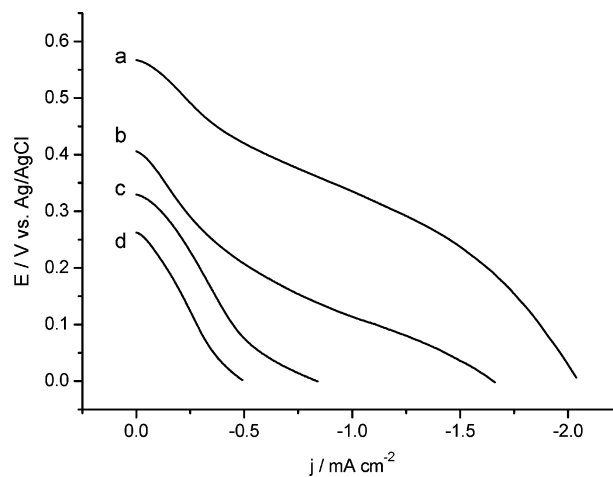


FIGURE 2. Galvanodynamic polarization plots of the electrocatalytic oxygen reduction at pyr-CoTMPP modified graphite foil (2 $\text{mg}_{\text{pyr-CoTMPP}}/\text{cm}^2$) in 0.5 M, oxygen saturated phosphate electrolyte solution, at (a) pH 2.4, (b) pH 4.5, (c) pH 7, and (d) pH 9.4. The solutions were stirred and purged with O_2 . The scan rate was 10^{-5} A s^{-1} .

to water or to hydrogen peroxide (Reactions 2–4). The consequence is a thermodynamically controlled shift of the polarization curve toward more negative values (Figure 2, curves a–d), which, depending on the nature and thus pH dependence of the anodic reaction, significantly reduces the MFC potential and power output. The observed potential shift should at room temperature ideally be 59 mV/pH, but as our data show, and as we have shown before (26), this dependence is found only at acidic pH values. At neutral pH, the slope is 29 mV/pH, which indicates a change of the nature of the rate-determining step, most probably from a $4 e^- / 4 \text{ H}^+$ (or $2 e^- / 2 \text{ H}^+$) to a $4 e^- / 2 \text{ H}^+$ (or $2 e^- / 1 \text{ H}^+$) reaction (relative to one oxygen molecule) (26).

Additionally to these thermodynamic effects the oxygen reduction kinetics depends on pH. Thus, the analysis of Tafel plots derived from the results of rotating electrode measurements also show a considerably slower rate of the oxygen reduction at neutral pH values. The exchange current density of the oxygen reduction, j_0 , measure of the kinetics of an electrochemical reaction, decreased at pyr-FePc modified electrodes from 60 $\mu\text{A cm}^{-2}$ (at pH 2.4) to 13 $\mu\text{A cm}^{-2}$ (at pH 7). This corresponds to a decrease of reduction rate of nearly 80%.

Effects of Electrolyte Concentrations. The polarization performance of the oxygen reduction catalysts is greatly influenced by the composition and the concentration of the cathodic electrolyte solution. During the oxygen reduction (following Reactions 2, 3, or 4) protons are consumed at the electrode surface. At increasing current densities this consequently leads to the formation of a pH gradient between the electrode surface and the bulk solution and to an increasing pH in the vicinity of the electrode surface and, consequently, to a shift of the potential of the oxygen reduction toward negative values. Therefore, the ability of the electrolyte to compensate these local pH changes, i.e., its buffer capacity, has a strong effect on the cathodic performance. This effect is illustrated in Figure 3. It shows, for the example of pyr-FePc in oxygen saturated electrolyte solutions, the dependence of the cathodic performance on the electrolyte composition and concentration. The main figure shows the current–potential behavior in differently concentrated phosphate electrolyte solutions (NaH_2PO_4 – H_3PO_4 , pH 3.3). At pH 3.3, this system has only a low buffer capacity ($\text{p}K_a(\text{H}_3\text{PO}_4) = 2.16$), and as expected, a lowering of the electrolyte concentration leads to strongly increasing impact of the proton consumption at the cathode surface due to the oxygen reduction.

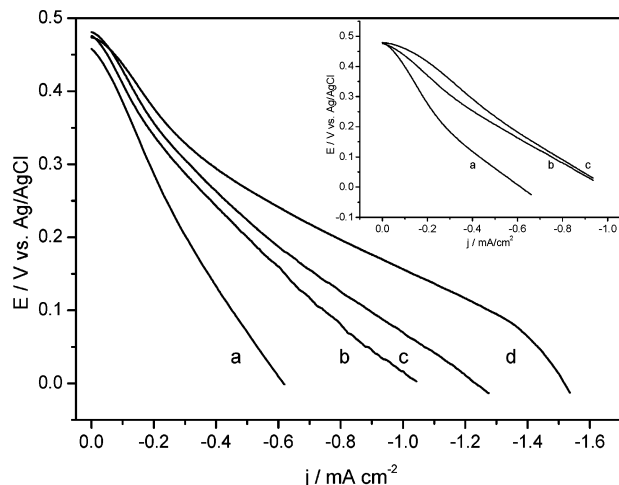


FIGURE 3. Galvanodynamic polarization plots of the electrocatalytic oxygen reduction at pyr-FePc modified graphite foil ($1 \text{ mg}_{\text{pyr-FePc}} \text{ cm}^{-2}$) in (a) 0.01 M, (b) 0.05 M, (c) 0.1 M, and (d) 0.5 M oxygen saturated pH 3.3 phosphate electrolyte solutions ($\text{NaH}_2\text{PO}_4\text{-H}_3\text{PO}_4$). Inset figure: The same experiment and pH as in the main figure, but performed in (a) 0.01 M, (b) 0.1 M, and (c) 0.5 M KNO_3 solution (the pH was adjusted with HNO_3). All solutions were stirred and purged with O_2 . The scan rate was 10^{-5} A s^{-1} .

TABLE 1. Summary of Limiting Oxygen Reduction Current Densities at 0 V (vs Ag/AgCl) for Pyr-FePc Modified Graphite Foil Electrodes (1 mg cm^{-2}), Derived from Galvano-dynamic Polarization Experiments (scan rate $10 \mu\text{A s}^{-1}$) in Different pH 3.3 Electrolyte Solutions

	oxygen purging mAcm^{-2}	air purging mAcm^{-2}
0.5 M phosphate electrolyte ^a	1.61 ± 0.13	1.25 ± 0.06
0.1 M phosphate electrolyte ^a	1.18 ± 0.10	0.97 ± 0.09
0.01 M phosphate electrolyte ^a	0.62 ± 0.08	0.58 ± 0.05
0.5 M NaCl ^b	1.01 ± 0.14	0.80 ± 0.09
0.5 M KNO_3 ^c	1.07 ± 0.11	0.86 ± 0.10
0.1 M KNO_3 ^c	0.98 ± 0.12	0.79 ± 0.11
0.01 M KNO_3 ^c	0.63 ± 0.05	0.55 ± 0.03

^a $\text{NaH}_2\text{PO}_4\text{-H}_3\text{PO}_4$. ^b pH was adjusted with HCl. ^c pH was adjusted with HNO_3 .

Since microbial fuel cells are usually operated using electrolyte solutions that possess low buffer capacities, such effect may severely limit the MFC performance. Nonbuffering electrolytes such as potassium nitrate cannot compensate these local pH gradients. Increasing electrolyte concentrations do not support high current densities (Figure 3, inset). The deviation of the polarization curve measured in 0.01 M solution is most likely caused by the increasing solution resistance and thus increasing potential drop (IR drop). At higher concentrations, IR effects were negligible.

These results are also reflected in the data presented in Table 1, which represent the limiting current densities that are achieved in galvanodynamic experiments performed in different electrolyte solutions and under air or oxygen purging. The data support the finding that only in sufficiently concentrated buffer solutions does the oxygen supply become limiting. In nonbuffering electrolytes or lower concentrated buffer solutions the difference between air and oxygen purged solutions strongly decreases.

These results are confirmed by microbial fuel cell polarization experiments that have been performed using the model MFC presented in Figure 4. As shown in Figure 5A for the example of pyr-FePc (all other materials showed a very similar behavior), the cathodic polarization curve shows a



FIGURE 4. Photograph of the batch-type microbial fuel cell setup. Cathode and anode compartment were equipped with reference electrodes. The cathode compartment was purged with air by means of a fish pump and a diffuser. Both compartments were stirred.

distinct shift toward more negative values when the concentration of the buffer solution (pH 7, $\text{NaH}_2\text{PO}_4/\text{Na}_2\text{HPO}_4$) in the cathodic cell compartment is decreased from 500 to 50 mM. As expected, near OCP, the difference is comparably low, but it reaches 61 mV at $100 \mu\text{A cm}^{-2}$.

The impact on the cell potential and the power curve (Figure 5B) is much more pronounced. At $100 \mu\text{A cm}^{-2}$, the cell potential decreases by 54% from 388 to 179 mV with decreasing buffer concentration, which goes along with the decrease of the power output from 2.3 to 1 mW. This additional effect has to be attributed to the increased resistance of the electrolyte solution and probably of the Nafion membrane at low ionic concentrations. It is not due to the establishment of a membrane potential across the Nafion membrane (due to concentration gradients between the anodic and the cathodic compartment). Such potential seems not to establish, probably because of a considerable flux of anionic and cationic species through the ion channels of the membrane.

The maximum power point, MPP, decreased by 35%, from 2.3 to 1.5 mW (11.5 mW L^{-1} and 7.5 mW L^{-1} , respectively). As it is illustrated in the figure, the decrease of the power output goes along with the shift of the MPP to higher external resistances. Since the maximum power point of current sources in DC circuits is generally found at $R_{\text{ext}} = R_{\text{int}}$ (derived from eq 1, a general description of the performance of power sources as a function of their internal resistance. See, e.g., ref 35).

$$P = \frac{E_0^2}{(R_{\text{ext}} + R_{\text{int}})} \quad (1)$$

(E_0 is the open circuit voltage, and R_{ext} and R_{int} represent the external load and the internal resistance, respectively.),

this shift means an increase of the internal resistance from approximately 60Ω to 200Ω .

As Figure 5 reveals, in comparison to the half cell (galvanodynamic) experiments as presented in Figure 3, the fuel cell passes its performance maximum well before the anodic or cathodic reaction reach mass transfer limitation. Thus, although the cathode is capable of reaching $600 \mu\text{A cm}^{-2}$ (in 50 mM, pH 7 solution) the power maximum of the model fuel cell is reached at only $70 \mu\text{A cm}^{-2}$. This result clearly shows the important issue of reducing the internal fuel cell resistance in order to achieve satisfactory fuel cell

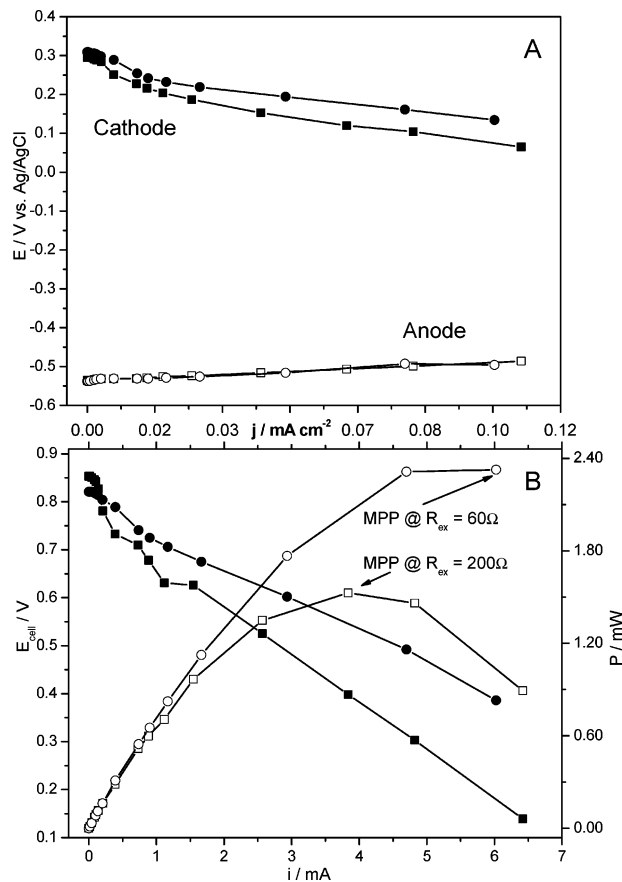


FIGURE 5. Microbial fuel cell experiment using an anaerobic culture of *Escherichia coli* K12 (substrate: 10 g L^{-1} glucose) in the anode chamber and differently concentrated (squares: 50 mM , circles: 500 mM phosphate buffer), air saturated pH 7 phosphate buffer solutions in the cathode chamber. The anode was a 100 cm^2 poly-(tetrafluoroaniline) coated platinum mesh (34), the cathode was a 60 cm^2 pyr-FePc modified graphite foil ($1 \text{ mg}_{\text{pyr-FePc}} \text{ cm}^{-2}$). **A:** Plot of the electrode potentials, measured versus Ag/AgCl reference electrodes in the anode and the cathode compartment; **B:** Polarization and power curves of the same experiment, derived from cell voltage and current (solid symbols: cell potentials (left axis); open symbols: power values (right axis)). The current density refers to the projected surface area of the cathode.

performance. As an example, the increasing resistance that is caused by the electrolyte solution can certainly be reduced by minimizing the distance between the anode and the cathode, while larger proton exchange membrane windows will decrease the resistance effect of the membrane (28, 36).

Effects of Catalyst Load. As eq 2 (simplified form of the Tafel equation) shows, the current density j of an electrochemical reaction is at low overpotentials proportional to the exchange current density j_0 , a measure of the electron-transfer kinetics (see above) and the concentration of species involved in the electrochemical reaction (37).

$$j = j_0 e^{\alpha z F \eta / RT} \quad (2)$$

(Where α is the symmetry factor of the electrochemical reaction, z is the number of transferred electrons, F is the Faraday constant, η is the overpotential, T is the temperature and R is the gas constant.)

For electrocatalytic reactions, j_0 is proportional to the rate of the electrocatalytic reaction and the number of electrochemically accessible catalytic centers. This proportionality vanishes at high overpotentials when mass transfer limits the current density. To improve the cathodic performance

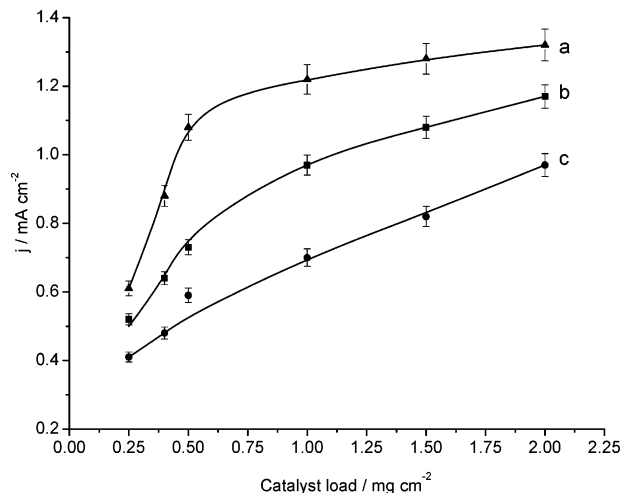


FIGURE 6. Plot of the oxygen reduction current density at a potential of 0 V measured at pyr-FePc cathodes as a function of the catalyst load and the composition of the electrolyte solution. (a) pH 3.3, 0.5 M phosphate ($\text{NaH}_2\text{PO}_4\text{-H}_3\text{PO}_4$), (b) pH 3.3, 0.1 M phosphate ($\text{NaH}_2\text{PO}_4\text{-H}_3\text{PO}_4$), and (c) pH 7, 0.1 M phosphate ($\text{NaH}_2\text{PO}_4\text{-Na}_2\text{HPO}_4$). The data were derived from galvanodynamic polarization experiments. All solutions were stirred and purged with air. The scan rate was 10^{-5} A s^{-1} .

under pH neutral conditions (where mass transfer limitations do not play a crucial role) the increase of the catalyst load represents an effective approach. Figure 6 shows the dependence of the current density on the catalyst load for different electrolyte solutions. As shown before, the electrode performance decreases with increasing pH and decreasing buffer concentration. A remarkable finding is that under acidic conditions (Figure 6, curve a) the current density reaches a plateau at a load of about 1 mg cm^{-2} , at which more than 90% of the maximum current density is achieved. The reason for this behavior is the limitation of the current by the mass transfer of oxygen to the electrode. 1 mg cm^{-2} catalyst load is sufficient to fully deplete the oxygen at the electrode surface. At lower electrolyte concentration and increasing pH (Figure 6, curve b, c) the oxygen supply becomes secondary. Here, the above-discussed local pH increase at the electrode surface, and the slower kinetics of the oxygen reduction limit the electrode performance. The increasing catalyst load increases the current density considerably (in pH 7 electrolyte solution nearly linearly). Consequently, the lack of performance under neutral pH in comparison to acidic conditions can be at least partially overcome by increasing the density of electrocatalytic centers. Thus, whereas at a load of 0.5 mg cm^{-2} the current density at pH 7 (0.1 M) was only 45% of that measured at pH 3, (0.5 M electrolyte), the ratio considerably improves at higher loads to reach 74% (0.97 mA cm^{-2}) at 2 mg cm^{-2} . The rather gentle slope of $0.4 \text{ mA/mg}_{\text{cat}}$ of the current increase (Figure 6, curve C) shows that a high percentage of catalytic centers are not electrochemically accessible or active. Optimized cathode preparation procedures will most likely help increasing this factor and result in a further improved cathode performance at lower catalyst loads.

As discussed above, the required cathode performance and thus necessary catalyst load mainly depend on the demands given by the MFC anode. Thus, Cheng et al. (5) have shown that a decreasing Pt load from 0.5 to 0.1 mg/cm^2 did not affect the power output of their microbial fuel cell. On the first glance, this finding seems contrary to our results. The analysis of the results of Cheng et al., however, reveals the following: In electrochemical experiments the authors reach current densities between 0.3 and 0.4 mA cm^{-2} at 0 V , which is in accordance with our data for low catalyst loads

(Figure 6, curve c). In their MFC experiments, the authors reach power densities of about $40 \mu\text{W cm}^{-2}$, which, at a cell potential of 500 mV, corresponds to a current density of $80 \mu\text{A cm}^{-2}$. This again is (in accordance with our findings) much lower than the possible current density at the cathode. It shows that, in this case, it is not the cathode that limits the fuel cell performance. Naturally, decreasing the catalyst load will not result in a decreasing MFC performance.

The Role of the Proton Exchange Membrane. The depletion of protons during the oxygen reduction is often given as an advantage over ferricyanide-based cathode systems, since it would allow preventing the acidification in the anode chamber. This, however, would require that the charge balancing ion transfer through the membrane from the anodic into the cathodic compartment is exclusively realized by a transfer of protons. The use of proton exchange membranes, e.g., of the Nafion type, may suggest that this is actually the case. As we have found in our study, and as it has already been reported (38), a transfer of alkali cations, such as Na^+ , takes place through the proton-exchange membrane. This cation transfer is caused by the insufficient concentration of protons in microbial fuel cells, which is orders of magnitude smaller than the concentration of, e.g., alkali cations. Thus, at pH 7, and using 50 mM phosphate buffer in the anodic compartment, the concentration of alkali cations is $5 \times E5$ times larger than the proton concentration. The diffusivity of protons through the PEM, however, is only 5 times higher than that of, e.g. sodium ions (39). As a measure of such transfer we analyzed the change of the pH in the cathode compartment during potentiostatically controlled microbial fuel cell experiments, in comparison to the measured electric charge. The flux of alkali cations in combination with the proton consumption during the oxygen reduction leads to the accumulation of hydroxide, and thus to a pH increase. For Nafion 117 membranes and in pH 7 0.1 M phosphate buffer (sodium salts) we found that at least 30% of the ion flux is due to alkali ion transfer. As the pH in the cathode compartment increases, the pH in the anodic electrolyte solution decreases. That means that in microbial fuels a situation arises in which in the course of the fuel cell operation, a significant pH gradient between the cathode and the anode may build up, which may lead to a decrease of microbial activity at the anode and the decrease of the oxygen reduction performance at the cathode. In such a case, active pH control, or the full abandonment of a cation exchange membrane and the use of air cathodes in membrane-less microbial fuel cells, (e.g., refs 27, 29, 31), may be necessary.

The present study reveals the limitations for oxygen cathodes in microbial fuel cells. Yet, these restraints are only of importance when limiting factors such as the internal fuel cell resistance are substantially reduced and higher MFC current and power densities are possible.

We show that even at low catalyst loads (0.25 mg cm^{-2}) of pyrolyzed iron phthalocyanine (pyr-FePc) current densities are achieved that are comparable to the current densities of platinum electrodes in other studies. Due to the low price of the noble metal free material, the catalyst load can be increased to achieve higher current densities when required.

The pH gradients between anodic and cathodic compartment caused during MFC operation in cation exchange membrane separated systems represents a severe problem that requires further discussions.

Acknowledgments

We gratefully acknowledge the support by the Office of Naval Research (ONR project N00014-03-1-0431), the Deutsche Forschungsgemeinschaft, and by the Fonds der Chemischen Industrie.

Literature Cited

- Uhlenbruck, S.; Tietz, F.; Haanappel, V.; Sebold, D.; Buchkremer, H.-P.; Stöver, D. Silver incorporation into cathodes for solid oxide fuel cells operating at intermediate temperature. *J. Solid State Electrochem.* **2004**, *8*, 923–927.
- Wang, S.; Lu, X.; Liu, M. Electrocatalytic properties of an $\text{Sr}_0.25\text{Bi}_0.5\text{FeO}_3\text{-d/LSGM}$ interface. *J. Solid State Electrochem.* **2001**, *5*, 375–381.
- Handbook of Chemistry and Physics*, 81 ed.; Lide, D. R., Ed.; CRC Press: Boca Raton, FL, 2000–2001.
- Rabaey, K.; Clauwaert, P.; Aelterman, P.; Verstraete, W. Tubular microbial fuel cells for efficient electricity generation. *Environ. Sci. Technol.* **2005**, *39*, 8077–8082.
- Cheng, S.; Liu, H.; Logan, B. E. Power densities using different cathode catalysts (Pt and CoTMPP) and polymer binders (Nafion and PTFE) in single chamber microbial fuel cells. *Environ. Sci. Technol.* **2006**, *40*, 364–369.
- Park, D. H.; Zeikus, J. G. Impact of electrode composition on electricity generation in a single-compartment fuel cell using *Shewanella putrefaciens*. *Appl. Microbiol. Biotechnol.* **2002**, *59*, 58–61.
- Park, D. H.; Zeikus, J. G. Improved fuel cell and electrode designs for producing electricity from microbial degradation. *Biotechnol. Bioeng.* **2003**, *81*, 348–355.
- Jasinski, R. Cobalt phthalocyanines as fuel cell cathode. *J. Electrochem. Soc.* **1965**, *112*, 526–528.
- Jasinski, R. A new fuel cell cathode catalyst. *Nature* **1964**, *201*, 1212–1213.
- Song, E.; Shi, C.; Anson, F. C. Comparison of the behaviour of several cobalt porphyrins as electrocatalysts for the reduction of O_2 at graphite electrodes. *Langmuir* **1998**, *14*, 4315–4321.
- Shi, C.; Anson, F. C. (5, 10, 15, 20-Tetramethylporphyrinato)-cobalt(II): A remarkably active catalyst for the electroreduction of O_2 to H_2O . *Inorg. Chem.* **1998**, *37*, 1037–1043.
- Ye, S.; Vijh, A. K. Oxygen reduction on an iron-carbonized aerogel nanocomposite electrocatalyst. *J. Solid State Electrochem.* **2005**, *9*, 146–153.
- Vasudevan, P.; Santosh; Mann, N.; Tyagi, S. Transition metal complexes of porphyrins and phthalocyanines as electrocatalysts for dioxygen reduction. *Trans. Metal Chem.* **1990**, *15*, 81–90.
- Mouahid, O. E.; Coutanceau, C.; Belgis, E. M.; Crouigneau, P.; Léger, J. M.; Lamy, C. Electrocatalytic reduction of dioxygen at macrocycle conducting polymer electrodes in acid media. *J. Electroanal. Chem.* **1997**, *426*, 117–123.
- Coutanceau, C.; El Hourch, A.; Crouigneau, P.; Leger, J. M.; Lamy, C. Conducting polymer electrodes modified by metal tetrasulfonated phthalocyanines: Preparation and electrocatalytic behaviour towards dioxygen reduction in acid medium. *Electrochim. Acta* **1995**, *40*, 2739–2748.
- Baranton, S.; Coutanceau, C.; Léger, J.-M.; Roux, C.; Capron, P. Alternative cathodes based on iron phthalocyanine catalysts for mini- or micro-DMFC working at room temperature. *Electrochim. Acta* **2005**, *51*, 517–525.
- Jahnke, H.; Schönborn, M.; G., Z. Organic dyestuffs as catalysts for fuel cells. *Topics Curr. Chem.* **1976**, *61*, 133–181.
- van Veen, J. A. R.; Colijn, H. A.; Baar, J. F. On the effect of heat treatment on the structure of carbon-supported metalloporphyrins and phthalocyanines. *Electrochim. Acta* **1988**, *33*, 801–804.
- Gojkovic, S. L.; Gupta, S.; Savinell, R. F. Heat-treated iron(III) tetramethoxyphenyl porphyrin chloride supported on high-area carbon as an electrocatalyst for oxygen reduction: Part II. Kinetics of oxygen reduction. *J. Electroanal. Chem.* **1999**, *462*, 63–72.
- Gouerec, P.; Savy, M.; Riga, J. Oxygen reduction in acidic media catalyzed by pyrolyzed cobalt macrocycles dispersed on an active carbon: The importance of the content of oxygen surface groups on the evolution of the chelate structure during the heat treatment. *Electrochim. Acta* **1998**, *43*, 743–753.
- Scherson, D.; Tanaka, A. A.; Gupta, S. L.; Tryk, D.; Fierro, C.; Holze, R.; Yaeger, E. B. Transition metal macrocycles supported on high area carbon: pyrolysis-mass spectrometry studies. *Electrochim. Acta* **1986**, *31*, 1247–1258.
- Lefèvre, M.; Dodelet, J. P.; Bertrand, P. O_2 reduction in PEM fuel cells: Activity and active site structural information for catalysts obtained by the pyrolysis at high temperature of Fe precursors. *J. Phys. Chem. B* **2000**, *104*, 11238–11247.
- Schulenburg, H.; Stankov, S.; Schünemann, V.; Radnik, J.; Dorbandt, I.; Fiechter, S.; Bogdanoff, P.; Tributsch, H. Catalyst for the oxygen reduction from heat-treated iron(III) tetramethoxyphenylporphyrin chloride: Structure and stability of active sites. *J. Phys. Chem. B* **2003**, *107*, 9034–9041.

- (24) Bogdanoff, P.; Herrmann, I.; Hilgendorff, M.; Dorbandt, I.; Fiechter, S.; Tributsch, H. Probing structural effects of pyrolysed CoTMPP-based electrocatalysts for oxygen reduction via new preparation strategies. *J. New Mater. Electrochem. Syst.* **2004**, *7*, 85–92.
- (25) Gojkovic, S. L.; Gupta, S.; Savinell, R. F. Heat-treated iron(III) tetramethoxyphenyl porphyrin chloride supported on high-area carbon as an electrocatalyst for oxygen reduction: Part III. detection of hydrogen peroxide during oxygen reduction. *Electrochim. Acta* **1999**, *45*, 889–897.
- (26) Zhao, F.; Harnisch, F.; Schröder, U.; Scholz, F.; Bogdanoff, P.; Herrmann, I. Application of pyrolysed iron(II) phthalocyanine and CoTMPP based oxygen reduction catalysts as cathode materials in microbial fuel cells. *Electrochem. Comm.* **2005**, *7*, 1405–1410.
- (27) Cheng, S.; Li, H.; Logan, B. Increased performance of single-chamber microbial fuel cells using an improved cathode structure. *Electrochem. Commun.* **2006**, *8*, 489–494.
- (28) Liu, H.; Cheng, S.; Logan, B. E. Power generation in fed-batch microbial fuel cells as a function on ionic strength, temperature, and reactor configuration. *Environ. Sci. Technol.* **2005**, *39*, 5488–5493.
- (29) Jang, J. K.; Pham, T. H.; Chang, I. S.; Kang, K. H.; Moon, H.; Cho, K. S.; Kim, B. H. Construction and operation of a novel mediator- and membrane-less microbial fuel cell. *Process Biochem.* **2004**, *39*, 1007–1012.
- (30) Hilgendorff, M.; Dorbandt, I.; Schulenburg, H.; Bron, M.; Fiechter, S.; Bogdanoff, P.; Tributsch, H.; Hahn-Meitner-Institut: Berlin, 2004; US2004236157, WO03004156.
- (31) Liu, H.; Logan, B. E. Electricity generation using an air-cathode single chamber microbial fuel cell in the presence and absence of a proton exchange membrane. *Environ. Sci. Technol.* **2004**, *38*, 4040–4046.
- (32) Schröder, U.; Nießen, J.; Scholz, F. A generation of microbial fuel cell with current outputs boosted by more than one order of magnitude. *Angew. Chem., Int. Ed.* **2003**, *115*, 2986–2989.
- (33) Rosenbaum, M.; Schröder, U.; Scholz, F. In situ electrooxidation of photobiological hydrogen in a photobiological fuel cell based on *Rhodobacter sphaeroides*. *Environ. Sci. Technol.* **2005**, *39*, 6328–6333.
- (34) Nießen, J.; Schröder, U.; Rosenbaum, M.; Scholz, F. Fluorinated polyanilines as superior materials for electrocatalytic anodes in bacterial batteries. *Electrochem. Commun.* **2004**, *6*, 571–575.
- (35) Lindner, H.; Brauer, H.; Lehmann, C. *Taschenbuch der Elektrotechnik und Elektronik*, 8. ed.; Fachbuchverlag Leipzig, 2004.
- (36) Oh, S.; Logan, B. Proton exchange membrane and electrode surface areas as factors that affect power generation in microbial fuel cells. *Appl. Microbiol. Biotechnol.* **2006**, *70*, 162–169.
- (37) Hamann, C. H.; Vielstich, W. *Elektrochemie*, 3. Auflage ed.; Wiley-VCH: Weinheim, 1998.
- (38) Gil, G. C.; Chang, I. S.; Kim, B. H.; Kim, M.; Jang, J. K.; Park, H. S.; Kim, H. J. Operational parameters affecting the performance of a mediator-less microbial fuel cell. *Biosens. Bioelectron.* **2003**, *18*, 327–334.
- (39) Stenina, I. A.; Sistas, P.; Rebrov, A. I.; Pourcelly, G.; Yaroslavtsev, A. B. Ion mobility in Nafion-117 membranes. *Desalination* **2004**, *170*, 49–57.

Received for review February 14, 2006. Revised manuscript received March 28, 2006. Accepted April 19, 2006.

ES060332P